# Solvation Dynamics by Computer Simulation: Coumarin C153 in 1,4-Dioxane

**Giorgio Cinacchi,† Francesca Ingrosso,* and Alessandro Tani‡**

*Dipartimento di Chimica, Università di Pisa, Via Risorgimento 35, I-56126, Italy*

*Received: March 17, 2006; In Final Form: May 10, 2006*

Computer simulation results are presented for an atomistic pair potential model of 1,4-dioxane which takes into account molecular flexibility. The model has been conceived to be applied to the study of solvatochromism and solvation dynamics in the presence of the polar probe coumarin C153. Computer simulations on the pure liquid have produced thermodynamical, structural, and dynamical data in good agreement with available experimental measures. This constitutes a valuable test of the 1,4-dioxane all-atom model employed. The study of solute−solvent interactions for C153 in 1,4-dioxane has been motivated by the aim of casting light, through simulations, on the interesting experimental findings according to which such a solvent behaves as a "polar" solvent with respect to dynamic solvation properties. Molecular dynamics is particularly suitable to model the process and provides an interpretation of the so-called "dioxane anomaly". An investigation of the structure of the solvation shell and of the dynamics of solvation is presented and discussed. In particular, the satisfactory accordance between simulated and experimental solvation response implies that the simulations give a reliable description of both solute and solvent at a molecular level and reinforces the idea that the explicit inclusion of discrete solvent molecules is needed for a realistic treatment of solvation phenomena in which the local structure of the liquid plays a key role.

## 1. Introduction

1,4-Dioxane (14DX) is a common solvent in chemistry. Its very low molecular electric dipole moment, $\mu$, and its dielectric constant, $\epsilon$, equal to 2.21, are very close to the corresponding properties of cyclohexane, isoelectronic with 14DX, and would naively lead to classify 14DX as a "nonpolar" solvent. However, 14DX behaves in many respects like solvents with a relatively large $\mu$ and $\epsilon$, which are therefore classified as "polar". For example, 14DX is completely miscible with water, and the two compounds demix only upon addition of a salt.[1]

Measurements of $^{131}$Xe quadrupolar NMR relaxation provide another example of the "1,4-dioxane anomaly". The relaxation rate of quadrupolar nuclei is determined by their interaction with the electric field gradient that, in the case of monatomic species, derives totally from the electrostatics of the solvent molecules. The relaxation rates of $^{131}$Xe in 1,3-dioxane and 1,4-dioxane are almost the same, despite the marked differences in the values of $\mu$ and $\epsilon$ of the two isomers[2]. To explain such a behavior, Monte Carlo (MC)[2] and molecular dynamics (MD)[3] simulations were performed employing site−site rigid nonpolarizable models of the two heterocycles. While the MD simulations were devoted to a direct comparison between calculated and experimental NMR observables,[3] the MC simulations were aimed at evaluating the electric field, **F**, felt by a dipolar solute (specifically 1,3-dioxane itself) in the two dioxane solvents.[2] The very similar results obtained show that the two isomers share a common behavior at a molecular level as far as electrostatic interactions are concerned, a finding in definite contrast with reaction field-based continuum theory predictions. The authors of refs 2 and 3 concluded that it is the full charge distribution of the solvent molecules that determines the relaxation rates of quadrupolar nuclei dissolved into them.

Analogous electric field calculations were performed in ref 4 by means of MD simulations employing united-atom rigid nonpolarizable models for the two dioxane isomers. In such a work, after equating the simulated **F** with the solvent reaction field, the Onsager expression was solved for $\epsilon$, thus obtaining a value of 7 for 14DX. This number was interpreted as the effective dielectric constant of 14DX, and it was proposed to use it in reaction field calculations of the solvatochromic shifts of polar solutes dissolved in this solvent. Indeed, the latter phenomenon constitutes a further example of the particular behavior of 14DX.

The solvatochromic shift of dipolar chromophores, like coumarin 153 (C153)[5,6] and 1-(9-anthryl)-3-(4-dimethylaniline) (ADMA),[7] dissolved in 14DX, was found to exceed continuum theory predictions. In addition, while the fluorescence decay of these solutes in nonpolar solvents is monoexponential, its profile is multiexponential in 14DX, as observed in polar solvents. Theoretical investigations showed that this is a consequence of the large quadrupole and higher order electrostatics.[7−9]

Solvatochromism and solvation dynamics in 1,4-dioxane cannot accurately be studied without using models explicitly taking into account the molecular detail and the local solvation structure, and therefore, a simple continuum model is not a valid means in this particular case.[6] To reproduce local interactions, an accurate description at a molecular level is necessary for both solute and solvent. Including nuclear relaxation represents a further step toward a realistic representation of dynamics, since conformational changes of the 14DX molecule could have an effect on the kinetics of charge transfer and solvatochromism occurring in solution.

Providing such an accurate model for solute and solvent to be used in molecular dynamics simulations has therefore

* To whom correspondence should be addressed. Present Address: Ecole Normale Supérieure, Département de Chimie, UMR 8640, 24 rue Lhomond, 75231 Paris Cedex 05, France. E-mail: fingross@gmail.com.

† E-mail: g.cinacchi@sns.it.

‡ E-mail: tani@dcci.unipi.it.

10.1021/jp0616765 CCC: $33.50 
Published on Web 06/17/2006

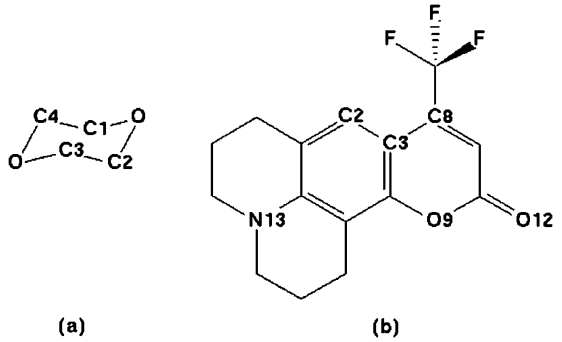


**Figure 1.** (a) 1,4-dioxane and (b) coumarin C153, with labels used in the text to indicate atomic sites. Hydrogen atoms are not depicted, but they are explicitly included in the calculations.

motivated this work. Quantum chemical calculations have been carried out to obtain optimized geometries for both solute and solvent, for which we have employed all-atomistic models. Partial flexibility was also included for both solute and solvent. Experimental measurements of solvatochromism and time-dependent fluorescence in 1,4-dioxane are available for coumarin C153.[5,6] We therefore have chosen C153 as a solute and used for it the parameters obtained in refs 10 and 11. Our analysis has been extended to a study of local properties related to solvation.

This paper is organized as follows. The all-atom models for solute and solvent molecules are described in section 2, along with the computational details of the simulations. To test the performance of the employed solvent model, we have first carried out MD simulations on the pure liquid 14DX. The presentation of calculated thermodynamic, structural, and dynamic quantities of pure 1,4-dioxane and their comparison with corresponding experimental data are reported in section 3. Solvation structure and dynamics in the presence of the probe C153 are presented in section 4 and ibidem the results for dynamics compared with experimental results. Conclusions are finally drawn in section 5.

## 2. Description of Solute and Solvent Models and Computational Details

Both solute and solvent molecules have been described at an all-atom chemically detailed level. The geometry optimization of a solvent molecule has been carried out with GAUSSIAN03[12] at the Hartree−Fock level using a 6-31G+(d,p) basis set, both in vacuo and in solution. Very small differences have been observed, most likely due to the low dielectric constant of the medium. The lowest energy conformation has been found to be the chair one, in agreement with previous quantum chemical calculations.[13] The optimized geometries are reported as Supporting Information (SupInf). In Figure 1a, we display the molecular structure of 14DX and the labels used in the following.

Internal flexibility for the solvent has been allowed with the exception of stretching (1,2) interactions, being the bond lengths constrained at the values given in Table 3 of the SupInf. As for the solute C153, shown in Figure 1b, the aromatic structure and the methylenic groups on the nonaromatic rings have been kept rigid, while stretching, bending, and torsion have been considered otherwise. The equilibrium geometries for the ground- and excited-state solute have been obtained elsewhere from quantum calculations,[10] and they are reported in Tables 5 and 6 of the SupInf.

Stretching (1,2), bending (1,3), and torsional (1,4) interactions have been evaluated according to the following formulas

$$U_{ij}^{1,2}(r) = \frac{1}{2}\kappa(r - r_0)^2 \quad (1)$$

$$U_{ijk}^{1,3}(\vartheta) = \frac{1}{2}K(\vartheta - \vartheta_0)^2 \quad (2)$$

$$U_{ijkl}^{1,4}(\varphi) = \frac{V_1}{2}(1 + \cos\varphi) + \frac{V_2}{2}(1 - \cos 2\varphi) + \frac{V_3}{2}(1 + \cos 3\varphi) \quad (3)$$

The parameters in eqs 1, 2, and 3 for the solvent have been extracted from the AMBER[14] and OPLS[15] force fields. They are listed in Table 4 of the SupInf.

As for the solute, we have employed parameters from the OPLS force field,[16,17] which are reported in Table 7 of the SupInf.

Intermolecular interactions between a molecule $I$ and a molecule $J$ have been represented by a sum of electrostatic and Lennard-Jones terms, as follows

$$U_{IJ}(r_{\alpha\beta}) = \sum_{\alpha\in I}\sum_{\beta\in J}\frac{q_\alpha q_\beta}{4\pi\epsilon_0 r_{\alpha\beta}} + 4\epsilon_{\alpha\beta}\left[\left(\frac{\sigma_{\alpha\beta}}{r_{\alpha\beta}}\right)^{12} - \left(\frac{\sigma_{\alpha\beta}}{r_{\alpha\beta}}\right)^{6}\right] \quad (4)$$

Each site bears a charge whose value for the solvent is listed in the second column of Table 8 of the SupInf. The charges of the solute sites have been computed in refs 10 (ground state) and 11 (excited state), and they are reported in Table 9 of the SupInf. Table 8 of the SupInf contains the values of the parameters $\epsilon$ and $\sigma$ for the solvent, taken from the OPLS force field,[15−17] while Table 10 of the SupInf contains the corresponding parameters for the solute, taken from ref 18. They represent the well depth and the contact distance between sites of the same type ($\alpha = \beta$), while, for a pair of unlike ($\alpha \neq \beta$) sites, these quantities have been evaluated according to standard combination rules.

The first MD run was started with a configuration of 125 14DX molecules placed in a simple cubic low-density structure that has completely melted and compressed after 2 ns of simulation performed in an isothermal−isobaric ensemble (MD-NPT) at a temperature $T = 298$ K and a pressure $P = 0.098$ MPa. The final configuration of this run served two purposes. First, it was replicated eight times in space to create a 1000 molecule configuration, with which to initiate a MD-NPT equilibration run of 1 ns. The latter was followed by a MD-NPT production run lasting 1 ns, during which configurations were saved every 1 ps to calculate thermodynamic and structural properties. Second, the above-mentioned 125 molecule configuration was used to begin an equilibration run in the microcanonical ensemble (MD-NVE) of 1 ns, followed by overall 8 ns of production in the same ensemble, during which averages of dynamic quantities were computed. In the center of the last configuration of the MD-NPT runs with 1000 14DX molecules, a spherical cavity was then created by removing 601 of them; one molecule of C153 was subsequently inserted in this cavity, thus generating the initial configuration of the MD-NVE simulation runs (2 ns of equilibration and 2 ns of data acquisition) aimed at calculating the C153 solvation structure and dynamics. The same procedure was adopted for the ground and excited state of the solute, and independent equilibrium simulations have been run in the two cases.

In all simulation runs, cubic boxes and standard periodic boundary conditions were used. The equations of motion were

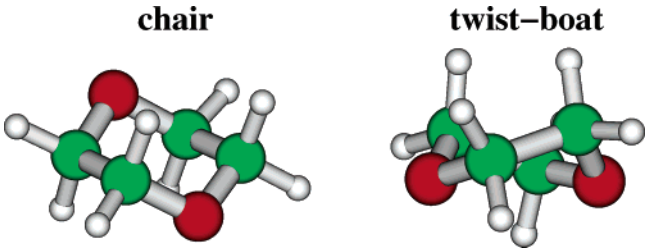


**Figure 2.** Examples of a chair and a twist-boat conformation of the 1,4-dioxane molecule.

integrated via the leapfrog version of the Verlet algorithm with a 2 fs time step. The constraints for the nonflexible parts of the solvent and of the solute structure were dealt with by using the SHAKE algorithm. The truncation of the Lennard-Jones interactions was treated by adding the usual long-range corrections. Neighbor lists were employed to speed up calculations. Electrostatic interactions were evaluated through the Ewald summation scheme. In the MD-NPT runs, the presence of an external mechanical and thermal bath was effectively mimicked according to the weak coupling method. The MD methodology just outlined is extensively described in ref 19.

## 3. Testing the Performance of the Solvent Model

**3.1. Thermodynamics.** The pressure, temperature, and density of the 1000 molecule MD-NPT production run were, respectively, $P = 0.1 \pm 10$ MPa, $T = 298 \pm 2$ K, and $\rho = 1.030 \pm 0.030$ g·cm$^{-3}$. The latter is in very good agreement with the corresponding experimental value of 1.0286 g·cm$^{-3}$.[20] The average intramolecular and intermolecular components of the potential energy were, respectively, $U_{intra} = 29.9 \pm 0.2$ KJ·mol$^{-1}$ and $U_{inter} = -38.1 \pm 0.2$ KJ·mol$^{-1}$. The latter value was split into $U_{qq} = -5.4 \pm 0.1$ KJ·mol$^{-1}$, the Coulombic contribution, and $U_{LJ} = -32.8 \pm 0.2$ KJ·mol$^{-1}$, with the contribution arising from the Lennard-Jones terms; thus, although the major contribution to the intermolecular potential energy comes from dispersion interactions, the electrostatic part is far from negligible (∼14%). The intra- and intermolecular components of the potential energy were used to estimate the enthalpy of vaporization, $\Delta H_{vap}$, according to the formula[15]

$$\Delta H_{vap} = U_{intra}(g) + RT - U_{intra}(l) - U_{inter}(l) \qquad (5)$$

The internal energy of the gas, $U_{intra}(g)$, was obtained by running a 1 ns MD simulation where all charges and Lennard-Jones parameters were set equal to zero, so that molecules can occupy the same point in space, and its value was $28.8 \pm 0.6$ KJ·mol$^{-1}$. Thus, the involved numbers lead to a value of $\Delta H_{vap}$ of $39.5 \pm 1$ KJ·mol$^{-1}$, in favorable agreement with its experimental counterpart, equal to 38.6 KJ·mol$^{-1}$.[20]

**3.2. Structure.** The molecular structure of 14DX was described by the method presented in ref 21. According to it, a conformation of a six-membered ring is identified by three variables: a total puckering amplitude, $Q$, and two angles, $\theta$ and $\phi$, which map any kind of conformation out onto a unit sphere. Thus, the two poles ($\theta = 0°$ and 180°) correspond to a chair conformation, while positions on the equator of the unit sphere correspond to boat or twist-boat conformations depending on the value of $\phi$ (see Figure 1 of ref 21). Two representative conformations of the 14DX molecule found during the course of the 1000 molecule MD-NPT production run are shown in Figure 2.

One can then define a properly normalized probability distribution function $\Pi(Q,\theta,\phi)$. From $\Pi(Q,\theta,\phi)$, a set of probability distribution functions can be derived by integrating on one or two variables among $Q$, $\theta$, and $\phi$. Since the longitude $\phi$ always turned out essentially equal to 90°, we can concentrate our interest in $P(Q,\theta)$ or in the two distributions derived from the latter, $P(\theta)$ and $P(Q)$. The latter functions are reported in Figure 3. $P(\theta)$ has a very prominent peak at $\theta = 0°$ (for symmetry reasons, only the boreal hemisphere is taken into consideration), while the inset highlights that a very low peak also exists at $\theta = 90°$. This means that 14DX molecules are almost always found in a weakly distorted 1,4 chair conformation, and only occasionally a 14DX molecule exists in a 2,5 twist-boat conformation (the 2,5 twist-boat conformation is identified by the values of the latitude, $\theta = 90°$, and of the longitude, $\phi = 90°$; see ref 21 for details). The contribution of 2,5 twist-boat conformations to the integral of $P(\theta)$ is ∼1%.

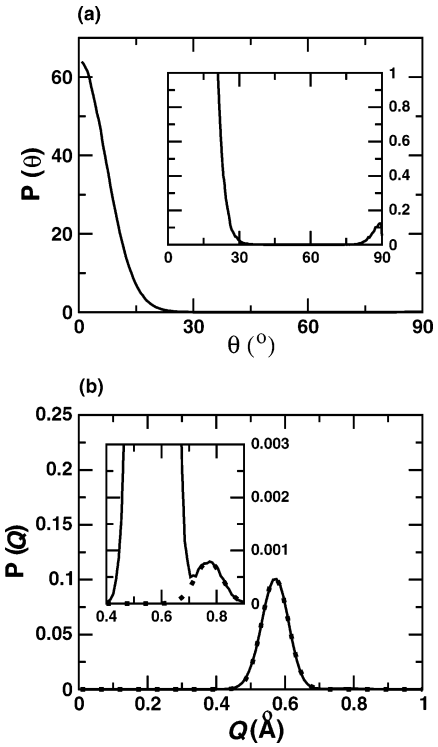


**Figure 3.** (a) Probability distribution function $P(\theta)$, with the inset showing details at very low function values. (b) The probability distribution function $P(Q)$, with the inset showing details at very low function values; dotted lines are Gaussian fits.

In ref 13, a quantum chemical conformational analysis of 1,4-dioxane was performed. It was found that the 1,4 chair conformation is the lowest in energy by all methods employed (HF/6-31G*, BLYP/6-31G*, and MP2/6-31G*). The other energy minima obtained corresponded to the 1,4 and 2,5 twist-boat conformations. They were found to possess almost the same energy with respect to that of the 1,4 chair conformation, ∼30 KJ·mol$^{-1}$. The most stable structure of the two depends on the method employed (HF predicts 1,4 while BLYP predicts 2,5; with the MP2 method, the same energy is obtained). Our simulated data are in qualitative accord with the theoretical results in that the probability of sampling a conformation other than a 1,4 chairlike one is very small, although the probability of finding a twist-boat conformation in the simulation is significantly higher than that deduced in the gas phase by the quantum chemical methods. In addition, only 2,5 twist-boat conformations were found in the simulations. These facts may indicate that the liquid phase tends to favor twist-boat conformations with respect to the gas phase, and, among them, the 2,5 over the 1,4. In Figure 3b, the distribution $P(Q)$ is plotted.

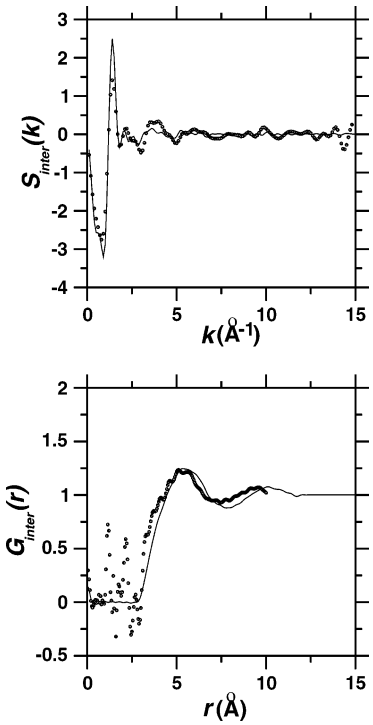


**Figure 4.** Experimental (dots) and simulated (solid lines) intermolecular structure factor $S_{inter}(k)$ and total pair correlation function $G_{inter}(r)$.

There is a first peak centered at $Q = 0.57$ Å, while the inset shows that a second very small peak exists at $Q = 0.77$ Å. By looking at the function $P(Q,\theta)$, the major peak can be related to the 1,4 chair conformations, while the minor peak corresponds to the 2,5 twist-boat conformations. The shape of the two peaks is Gaussian, with an amplitude of 0.16 Å for the higher and 0.19 Å for the lower. The value of the total puckering amplitude $Q = 0.57$ Å is in very good agreement with the experiments. In particular, the accord is quantitative with the result of an electron diffraction study,[22] while X-ray diffraction[23] and liquid crystal NMR[24] measurements reported values of 0.56 and 0.55 Å, respectively.

Both X-ray and neutron diffraction measurements provide experimental information on the structure of a liquid. In the former case, this information is deduced from the structure function, $S_X(k)$, a sum of the Fourier transforms of the total site−site correlation functions weighted by the X-ray scattering factors. $S_X(k)$ can be further decomposed into intra- and intermolecular contributions. From the latter, $S_{inter}(k)$, the experimental intermolecular total pair correlation function is obtained according to

$$G_{inter}(r) = 1 + \frac{1}{2\pi^2 r \rho_s} \int_0^\infty k S_{inter}(k) \sin(kr)\, dk \qquad (6)$$

with $\rho_s$ the number density of the sites. In Figure 4, the experimental $S_{inter}(k)$ and $G_{inter}(r)$[23] are compared with the corresponding simulated quantities. The agreement between the two sets of data is reasonable.

In neutron diffraction experiments of molecular liquids, the experimental structure factor, $S_N(k)$, is split into an intramolecular, $f_I(k)$, and a intermolecular, $D_M(k)$, contribution. $kS_N(k)$ is then Fourier transformed to give

$$d(r) = \frac{2}{\pi} \int_0^\infty k S_N(k) \sin(kr)\, dk \qquad (7)$$

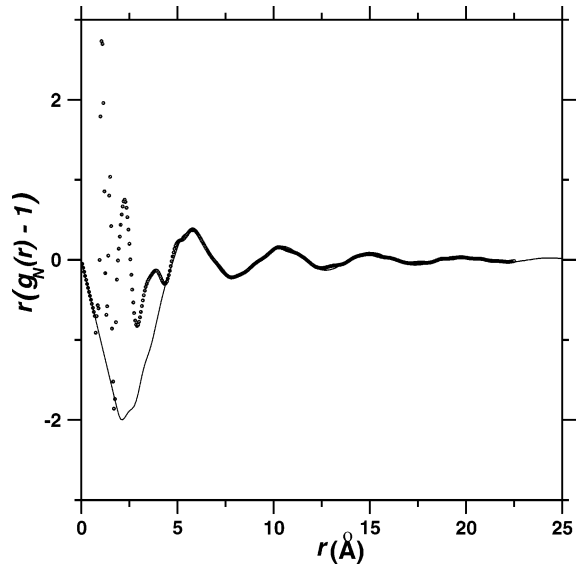


**Figure 5.** Comparison between neutron diffraction total pair distribution function (dots) and the intermolecular part of the corresponding function calculated from simulation (solid line).

The function $d(r)$ is related to the function $g_N(r)$ through the relationship

$$d(r) = 4\pi r \rho_M (g_N(r) - 1) \qquad (8)$$

with $\rho_M$ the molecular number density. In turn, $g_N(r)$ is a weighted sum of the atom−atom radial distribution function, $g_{\alpha\beta}(r)$

$$g_N(r) = \frac{\sum_\alpha \sum_\beta x_\alpha x_\beta b_\alpha b_\beta g_{\alpha\beta}(r)}{\sum_\alpha \sum_\beta x_\alpha x_\beta b_\alpha b_\beta} \qquad (9)$$

with $x_\alpha$ and $b_\alpha$ being the molar fraction and the scattering length of site α, respectively. The latter functions are not experimentally available for 14DX. In Figure 5, the function $r(g_N(r) - 1)$ obtained from the experiments[25] is compared with the intermolecular part of the corresponding function calculated from the simulation. (Of course, since neutron diffraction experiments were conducted on the per-deuterated 1,4-dioxane liquid, we have used the appropriate scattering length of the deuterium in the calculations.) The agreement is good, apart, of course, at short distances, dominated by the intramolecular peaks (see also Figure 4 of ref 25).

The satisfactory agreement between simulated structure functions and the corresponding quantities measured in diffraction experiments allows us to characterize further the structure of the liquid with confidence. Although atom−atom radial distribution functions constitute the more detailed knowledge available, prompter pieces of information are obtainable if we adopt a "molecular" point of view, according to which a 14DX molecule is seen as a globular particle with two embedded dipoles, respectively, formed by the two $CH_2-O-CH_2$ groups.

The center of mass pair distribution function obtained from simulation is shown in Figure 6. The shape of $g_{CM}(r)$ much resembles that of an atomic van der Waals liquid, with the first shell coordination number being ≈13. (This result was also obtained in ref 26, where a MC simulation on a pure system of rigid nonpolarizable 14DX model molecules was carried out.)

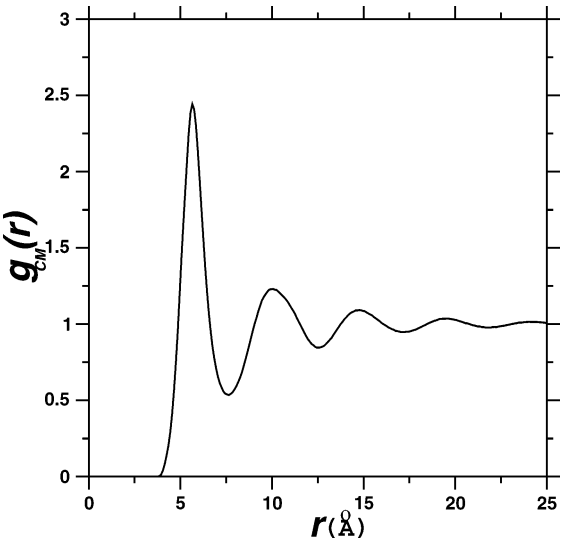


**Figure 6.** Center of mass pair distribution function of the simulated 1,4-dioxane liquid.

Thus, as far as translational order is concerned, 14DX is nothing other than an ordinary liquid.

It is not ordinary, however, from the orientational order point of view. Orientational order in a molecular liquid can be described by means of the following correlation functions

$$G_l(r) = \langle P_l(\cos \gamma(r)) \rangle \tag{10}$$

with $P_l()$ being the Legendre polynomial of $l$th rank and $\gamma(r)$ the angle between two particular vectors of two molecules separated by a distance $r$. Usually, $l = 1$ and $l = 2$ are considered. In the present work, the molecular vectors taken into consideration are, respectively, the vector joining the two oxygen atoms and the dipole moment of a $CH_2-O-CH_2$ group. The angular correlation functions $G_1(r)$ and $G_2(r)$ for these two vectors are plotted in Figure 7.

The OO vector shows, of course, no head-to-tail symmetry ($G_1(r)$ in Figure 7a is essentially equal to zero at all $r$) and just a modest degree of alignment at short range (notice the structure of $G_2(r)$ at $r$ less than $\approx$7 Å in Figure 7b). Conversely, the $CH_2-O-CH_2$ dipole of two molecules strongly aligns antiparallel at very short range, as revealed by the well equal to $-0.46$ at 3.4 Å in the function $G_1(r)$ of Figure 7c. It is this first shell structure that any solute dissolved in 14DX mostly probes, as it will be seen in the case of C153 presented below.

**3.3. Dynamics.** In the following, we present the results for two single-molecule properties, that is, mean square displacement (msd) and velocity autocorrelation function (acf), which yield the translational diffusion coefficient ($D$), and for the reorientational time correlation functions, which probe the time dependence of orientational correlations. Shear and bulk viscosity results are also provided to test collective dynamics.

The raw data used to compute the reported quantities were obtained in four independent runs, each spanning 2 ns of system time, and carried out in the microcanonical ensemble in order not to affect particle dynamics. Green−Kubo relations have been employed to compute $D$ (as the time integral of the velocity acf) and shear viscosity (from the acf of the off-diagonal elements of the stress tensor), as well as bulk viscosity (where a proper combination of the acf of diagonal elements is required, see, for example, ref 27).

Both msd and the velocity acf lead to the same value of $D$, namely, $(0.78 \pm 0.01) \times 10^{-5}$ cm$^2$/s at a translational temperature of 291 K. The corresponding experimental result is a bit larger, $0.89 \times 10^{-5}$ cm$^2$/s at 288 K.[28]

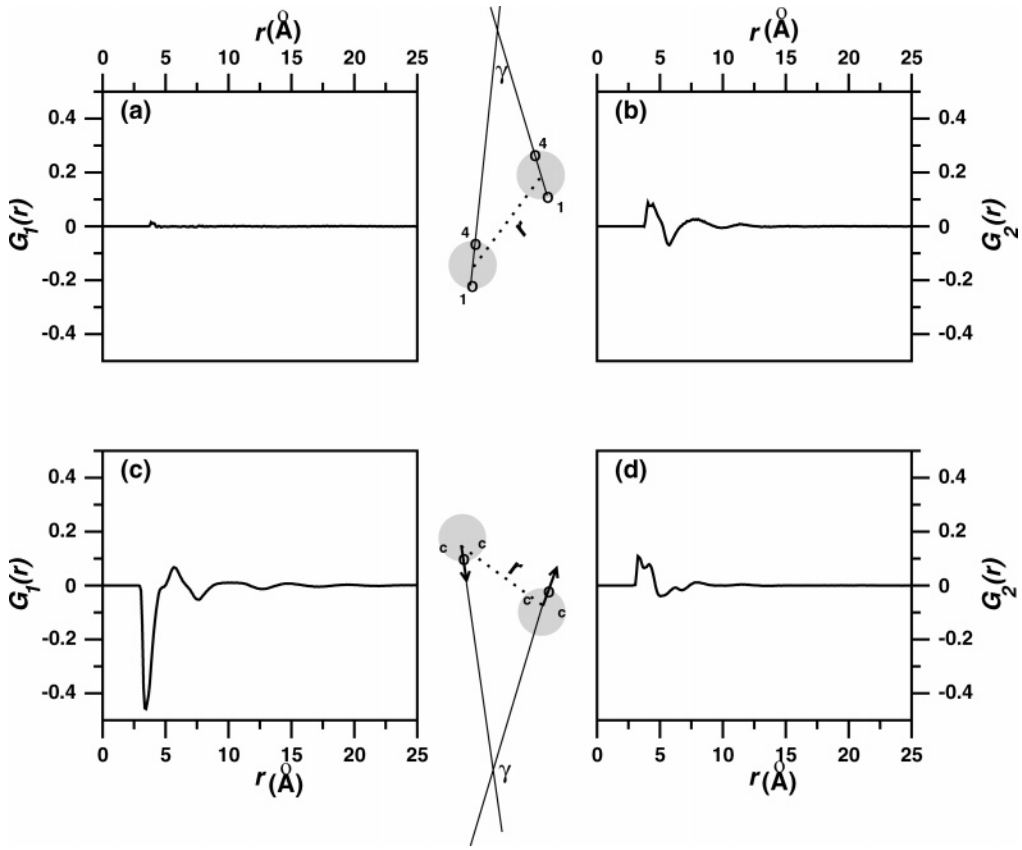


**Figure 7.** Orientational correlation functions in liquid 1,4-dioxane: (a) $G_1(r)$ of the OO vector, (b) $G_2(r)$ of the OO vector, (c) $G_1(r)$ of the $CH_2-O-CH_2$ dipole, and (d) $G_2(r)$ of the $CH_2-O-CH_2$ dipole. The pictures at the center of the figures define the quantities involved.

**TABLE 1: Parameters Used to Fit the Orientational Time Correlation Functions**

| parameters[a] | $P_1$ | $P_2$ |
|---|---|---|
| $a_1$ | 0.79 | 0.30 |
| $\tau_1$ (ps) | 8.43 | 5.56 |
| $a_2$ | 0.13 | 0.44 |
| $\tau_2$ (ps) | 2.72 | 2.05 |
| $a_3$ | 0.08 | 0.26 |
| $\tau_3$ (ps) | 0.39 | 0.35 |

[a] The orientational time correlation functions $P_1(x(t))$ and $P_2(x(t))$ (with $(x(t)$ defined in the text) were calculated during the MD-NVE simulations. The function used for the fit is a sum of three exponentials: $f(t) = a_1e^{-t/\tau_1} + a_2e^{-t/\tau_2} + a_3e^{-t/\tau_3}$. Notice that $a_1 + a_2 + a_3 = 1$ has been adopted.

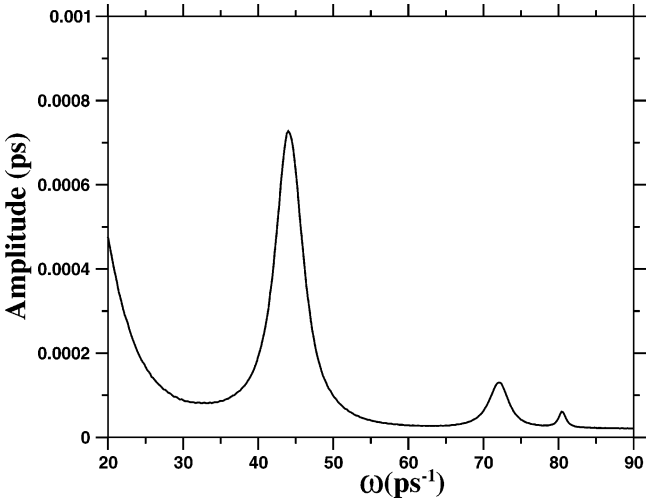


**Figure 8.** Power spectrum of $P_1(x(t))$ in the high-frequency region. $x(t)$ is defined in the text.

Orientational relaxation has been monitored via the decay of the functions $P_1(x(t))$ and $P_2(x(t))$ where $x(t) = \langle \mathbf{e}(0)\cdot\mathbf{e}(t)\rangle$, with $\mathbf{e}(t)$ being a unit vector in, or normal to, the average plane of the four carbon atoms of the molecule. The orientational correlation functions have been fitted with a three-exponential function, and the results for the case $\mathbf{e}(t)$ normal to the above-mentioned plane are collected in Table 1. The results for the vector $\mathbf{e}(t)$ in the above-mentioned plane are quite similar.

A single relaxation time is reported in experimental studies with depolarized Rayleigh scattering[29] or Raman spectroscopy[30,31] techniques, and this is ~3 ps at 298 K, significantly smaller than our longest relaxation time. Fitting our $P_2$ data with a single exponential yields a correlation time of 2.3 ps; the quality of the fit, however, is greatly worsened, which seems to indicate that more than one relaxation channel is present in the orientational dynamics of 14DX. The only physical feature missed by the three-exponential model is a very feeble oscillation at very short time. This is more easily visible in the power spectrum of $P_1(x(t))$ shown in Figure 8. The most intense signal is centered at $\simeq$44 ps$^{-1}$. This is presumably due to a librational motion of the tagged molecule, as no such oscillation is apparent in the center of mass velocity acf.

The computed shear viscosity at 298 K is 1.45 $\pm$ 0.3 mPa·s and overestimates a bit the values of 1.18 and 1.17 mPa·s measured, respectively, in ref 32 and ref 33. As to bulk viscosity, we have obtained a value of 12.3 $\pm$ 1.2 mPa·s. Bulk viscosity is roughly 1 order of magnitude larger than shear viscosity, in agreement with the general trend exhibited by this property; however, we are not aware of any experimental data for 14DX bulk viscosity to compare directly with our data. The overall picture of the solvent dynamics provided by the model indicates slightly slower translational and rotational motions compared with the experimental data.

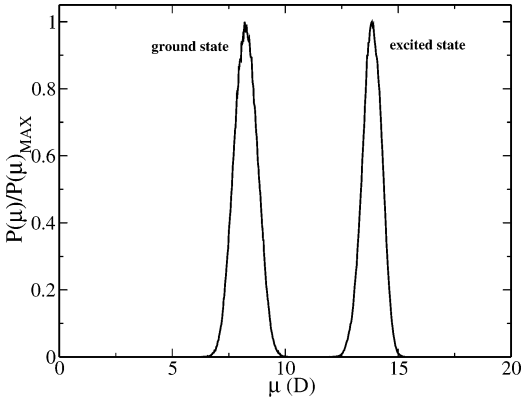


**Figure 9.** Normalized distribution of solute dipole moment in solution.

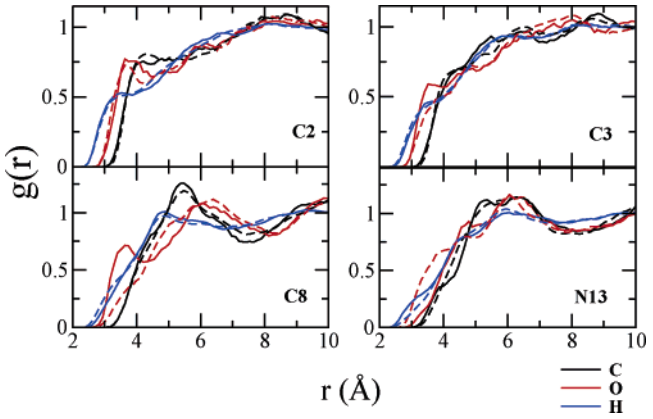


**Figure 10.** Solute−solvent site−site pair correlation functions for four C153 sites (see Figure 1 for labeling). The ground-state results are shown in full lines, while the excited-state results are shown in dashed lines.

## 4. C153 in 1,4-Dioxane

**4.1. Static Properties.** We start the discussion of our results by considering average changes on the solute when it is immersed in 1,4-dioxane. In particular, we consider the effect on the molecular dipole moment. We recall here that this property is subject to changes during the simulation, because the geometry is flexible. The charge distribution on C153 in the ground state leads to a dipole moment of 6.9 D for the isolated molecule. We have calculated the distribution of dipole moment intensity from the simulated trajectory, and the normalized function is reported in Figure 9.

As shown in this figure, the maximum for the dipole distribution in the ground state is located around 8.2 D. A similar behavior was observed by immersing C153 in polar solvents.[10,34] Analogous effects were also found for the excited state, even though much less pronounced (dipole for the isolated molecule, 13.4 D; position of the maximum in the normalized distribution of dipole intensities, 13.9 D).

Let us take a closer look at the solvation structure. In Figure 10, we report the solute−solvent pair correlation functions for four C153 sites in the ground and in the excited state. The choice of these particular sites will be more clear in the discussion of orientational correlations presented below.

According to our results, changes in the solvation shell of C153 in going from ground to excited state are not drastic. Some pair correlation functions change in shape, and some of them suggest a slightly different arrangement of solvent molecules

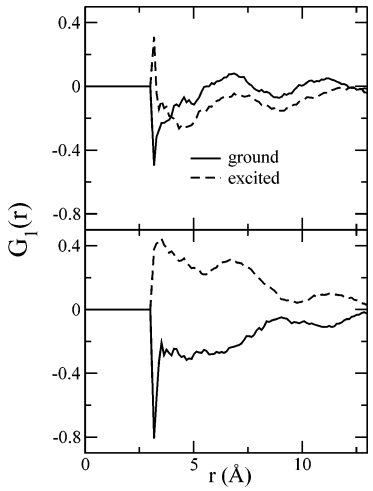


**Figure 11.** Solute−solvent orientational correlations for C153 in dioxane. Correlation is between the $CH_2-O-CH_2$ direction in the solvent and the two directions in the solute, defined in the text. The top panel refers to the N13−C2 direction, while the bottom panel refers to the C3−C8 direction.

in the two cases. For example, in the C8−O pair correlation function, at distances corresponding to the first solvation shell, slightly smaller values are associated with the excited-state result. This might be interpreted in terms of changes in the atomic partial charges.[10] The solvent oxygen atoms bear a negative charge, and the C2 atom becomes more negative in the excited state than it is in the ground state (see SupInf). Similar considerations can be made for the C3−O and the C2−O functions, while the opposite is true for N13−O (N13 becomes more positive).

We also studied dipolar orientational correlations between solute and solvent to analyze the orientation of solvent molecules around the solute.[10]

Since the charge-transfer excitation in the solute molecule occurs as a charge flux from the donor group (amino-group) to the acceptor group ($-CF_3$) through the $\pi$ electrons of the aromatic rings, we chose two representative directions in the C153 molecule, N13−C2 and C3−C8 (see Figure 1b). This gives more information about the molecular structure and charge distribution of C153 than just considering the direction of the molecular dipole moment. We therefore studied the relative orientation of each of the unit vectors along these two directions and a unit vector along the direction of the dipole moment of the $CH_2-O-CH_2$ group. Referring to eq 10, the angle $\gamma$ that is monitored in this case is the one formed by either the N13−C2 or the C3−C8 direction and the local dipole in the solvent. The distance between the two unit vectors is taken from the position of the center of mass of the system formed by the two solute atoms and the center of mass of the $CH_2OCH_2$ group. The results are shown in Figure 11.

In the ground state, orientational ordering is consistent with an average antiparallel orientation of solvent local dipoles with respect to both solute internuclear vectors in the first solvation shell, as shown from the negative value of the first peak of the $G_1$ function for both the considered directions. We observe that a larger orientational order can be explained on the basis of the polarity along the C3−C8 and N13−C2 directions. A larger charge difference is observed between sites N13 and C2 compared with that between C3 and C8. This leads to stronger dipolar interactions with the partial solvent dipole. After excitation of the solute, the polarity along both the C3−C8 and the C2−N13 directions changes and the average orientation in the first solvation shell becomes parallel in both cases. The charge difference between C3 and C8 and between C2 and N13 becomes much more similar than it is in the ground state, and as a consequence, also the orientational ordering in the first solvation shell is more similar.

We therefore observed smaller changes in the solvation shell description obtained from solute−solvent pair correlation functions than we did for orientational ordering. Thus, it appears that changes in the solvation shell around the ground- and the excited-state solute occur mostly as changes in the orientation of the solvent molecules, and smaller changes are associated with an increase/decrease of the solvation coordination number (and radial distance). This finding is in agreement with results obtained from molecular dynamics simulations of C153 in other polar fluids.[10,11]

**4.2. Solvatochromism and Solvation Dynamics.** Under the assumption that the variation of the solute geometry is negligible in the excitation process, the solvatochromic shift in a polar solvent can be defined in terms of the difference in the solute Hamiltonian between the excited and the ground state, which is related to the difference in solute−solvent interaction energy $\Delta E$.

When the main contribution to the solute−solvent intermolecular potential is electrostatic, $\Delta E$ can be evaluated according to[10]

$$\Delta E(r_{\gamma,j\eta}) = \sum_{j=1}^{N_{\mathrm{solv}}} \sum_{\gamma\in\mathrm{sol}} \sum_{\eta\in\mathrm{solv}} \frac{\Delta q_\gamma q_{j\eta}}{4\pi\epsilon_0 r_{\gamma,j\eta}} \tag{11}$$

where the sum over $j$ runs over $N_{\mathrm{solv}}$ solvent molecules, $\gamma$ is a solute site, and $\eta$ is a solvent site. The difference $\Delta q_\gamma$ is calculated between the partial charge on the solute site $\gamma$ in the excited and in the ground state, while $q_{j\eta}$ is the partial charge of the site $\eta$ in the solvent molecule $j$.

Under the linear response approximation (LRA), the equilibrium fluctuations of $\Delta E$ with respect to its average value ($\delta E(t) = \Delta E(t) - \langle \Delta E \rangle$) can be used to calculate the solvation response function SRF($t$) generated in the perturbed system, that is, the solvent exposed to a sudden change of the solute charge distribution as a consequence of the excitation. This is accomplished by calculating the normalized time correlation function (TCF) of the fluctuations in the ground (0) and in the excited (1) state[35]

$$\mathrm{SRF}(t) \cong \frac{\langle \delta\Delta E(0)\cdot\delta\Delta E(t)\rangle_{0,1}}{\langle |\delta\Delta E(0)|^2\rangle_{0,1}} \tag{12}$$

where $\langle\cdots\rangle$ indicates that the equilibrium ensemble average is performed in the unperturbed (ground or excited state) system. The SRF($t$) function is the theoretical counterpart of the experimental time-dependent Stokes shift[36] in the linear response approximation.

The Stokes shift for the $\pi \rightarrow \pi^*$ transition of C153 can be also evaluated from simulation as the difference between the absorption and emission shifts

$$\Delta\Delta\nu = \Delta\nu_{\mathrm{abs}} - \Delta\nu_{\mathrm{em}} \tag{13}$$

which can be computed as[37]

$$h\Delta\nu_{\mathrm{abs(em)}} = \langle \Delta E \rangle \tag{14}$$

where the symbol $\langle\ \rangle_n$ defines equilibrium averages over the ground ($n = 0$) or the excited ($n = 1$) state trajectories.

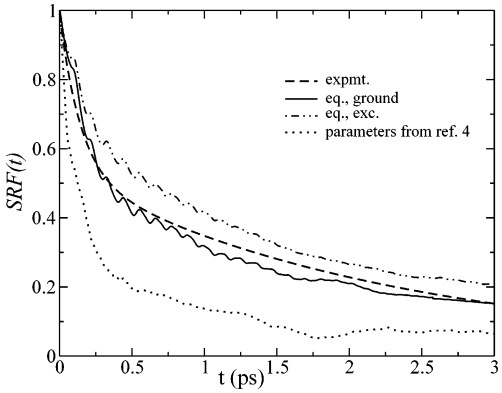


**Figure 12.** Calculated (full, dot−dashed, and dotted lines) and experimental[5] (dashed line) solvation response function.

The equilibrium probability distributions of $\Delta E_{0(1)}$ were Gaussian and centered at 1670 $cm^{-1}$ (0) and 2810 $cm^{-1}$ (1). Thus, the shift of the absorption is equal to 1670 $cm^{-1}$, while the corresponding shift for the emission is 2810 $cm^{-1}$, from which we obtain a Stokes shift of 1140 $cm^{-1}$ (the error associated with the calculation is 200 $cm^{-1}$). The experimental estimate[38] is 1240 cm $^{-1}$ (the uncertainty is 100 $cm^{-1}$). On the basis of the reasonable agreement found between experiments and computer simulations, we can state that the picture of solvatochromism obtained with our model seems to be correct and the peculiar behavior of 1,4-dioxane as "polar" solvent is well reproduced.

The next step is to describe the dynamics of solvation, according to the information contained in the SRF(*t*) function defined in eq 12. In Figure 12, the calculated result is shown and compared with the experimental one.[5]

The experimental result from ref 6 lies between the ground and the excited-state result. However, the agreement between calculation and experiment is reasonable. The calculated functions are well fitted by a combination of two exponentials. The fastest one dominates the response both in the ground and in the excited state (69% and 63% of the overall response, respectively), and the relaxation times are 0.122 ps in the ground state and 0.400 ps in the excited state. The slower exponential relaxation times are 2.670 and 3.680 ps, respectively. The experimental function was fitted by using three exponentials. However, the slowest one (with a relaxation time of 18.3 ps) accounted only for 2% of the total response. The exponential with an intermediate relaxation time (2.21 ps) was 52% of the total response, while the fastest one (0.177 ps) was 46% of the total response.

Usually, different decay rates between the ground and the excited-state results are interpreted as an indication of deviation from linear response.[39] However, in the present case, differences between the two functions are within the error associated with the simulation (20%). Calculation of the nonequilibrium solvation response[39] would help in the interpretation of the results. Nonetheless, such a calculation requires a much larger computational effort, and it is beyond the scope of the present work.

In the calculated response, an oscillatory feature can be observed, probably related to libration motions of the solvent, as suggested by its frequency, that is the same as that of the pure solvent, shown in Figure 8. This behavior of the computed SRF(*t*) has already been found in other systems.[10,40] We have shown[40] that it is not possible, with the accuracy associated with the experimental measurements, to obtain such a feature from the measured time-dependent function.

As a final remark of the present section, we would like to stress the importance of a realistic potential and molecular shape to reproduce time-dependent properties such as the solvation response function. In Figure 12, we display the SRF(*t*) for a ground-state equilibrium simulation of C153 in 14DX, where we used the solvent parameters from a united-atom rigid model given in ref 4. The parameters for the solute are the same as those described in section 2. The solvation response is considerably faster than it should be, possibly due to a less accurate description of the dynamics arising from interaction of a solvent molecule in the cage formed by its nearest neighbors. This would result in smaller torques exerted on the molecule and therefore in faster motion in the cage. However, also the small time scale results differ, which seem to suggest that the united-atom model does not reproduce correctly the inertial/rotational behavior of 14DX.[41]

The calculation of solvatochromism and solvation dynamics that we performed are based on eq 11, which, as already pointed out, only considers the electrostatic contribution to the solute−solvent interaction energy. This needs to be taken into account when considering the agreement that we found with experiment. Nonetheless, eq 11 has been widely used in molecular-dynamics-based studies of solvations dynamics in low-polarity solvents.[8,9,35,42,43] Calculations of solvation dynamics from nonequilibrium molecular dynamics simulations are also necessary to verify the agreement with experiment.

## 5. Conclusions

We have presented a study of structural and dynamical properties related to solvation of coumarin C153 in 1,4-dioxane.

The starting point of such a study has been the development of a pair potential for liquid dioxane capable of a realistic representation of its geometric structure as well as its liquid-state properties, both from the static and the dynamic points of view. Simulation runs on the pure liquid have produced data in good agreement with available experimental data. In addition, an investigation of the orientational order in liquid 1,4-dioxane has been carried out, with the scope of investigating the local structure of the liquid and to relate it to the peculiar properties of 1,4-dioxane with respect to solvation.

The next step has been running molecular dynamics simulations in the presence of the polar solute C153. This has allowed us to analyze the structure of the solvation shell, in particular by investigating solute−solvent orientational correlations, and to characterize the solvation response to electronic excitation in the solute. Comparison of the dynamics results with experiments has given satisfactory agreement. Our model is therefore able to give a realistic description of 1,4-dioxane, and it reasonably reproduces properties depending on the local structure, which is presumably related to the so-called "dioxane anomaly".

The results obtained for the C153−14DX system suggest a few comments with which we would like to end the present work. It appears that solvent molecules need to be explicitly and distinctly taken into account if a realistic picture of the solvation phenomenon at a molecular level is sought for. The drawbacks of solvation continuum theories in the special case of 1,4-dioxane solvent may hint that results from a simplified version of such theories (nonrealistic solute cavity, neglecting the inclusion of explicit solvent molecules in case of specific interactions, etc.) might be found to be misleading, even in those cases, like polar solvents, where they are in agreement with experimental findings. In fact, one cannot exclude the possibility that successful comparisons hide a compensation of errors in the theory. In this respect, a parallelism exists between the structural and dynamical behavior of a dye probe in isotropic

solvents and the ordering of rigid solutes in nematic liquid-crystalline solvents. In both cases, continuum theories have been formulated to explain experimental data; the reader is, respectively, referred to ref 44 and ref 45. Although many are the examples where these theories are successful, there are significant examples in which they inevitably fail. The approaches that seem to not exhibit such shortcomings have a unique feature in common: they handle solute−solvent interactions at a molecular level. From this point of view, the results presented in this work provide an example of the first case, while, for the case of the ordering of rigid solutes in nematic solvent, the work carried out in ref 46 is particularly representative. Experimental studies on solvation dynamics of dye probes in the isotropic phase of nematogenic materials have been recently carried out.[47] It would be interesting to supplement them with MD computer simulations.

**Acknowledgment.** We are grateful to Dr. Imre Bakó (Hungarian Academy of Sciences, Budapest) for sending us his experimental diffraction results on liquid 1,4-dioxane. All authors have contributed equally to this work.

**Supporting Information Available:** The complete citation for ref 12, solute and solvent optimized geometries, and the other potential parameters used in this work are presented. This material is available free of charge via the Internet at http://pubs.acs.org.

## References and Notes

(1) Takamaku, T.; Yamaguchi, A.; Matsuo, D.; Tabata, M.; Yamaguchi, T.; Otomo, T.; Adachi, T. *J. Phys. Chem. B* **2001**, *105*, 10101.
(2) Luhmer, M.; Stien, M.; Reisse, J. *Heterocycles* **1994**, *37*, 1041.
(3) Luhmer, M.; Reisse, J. *J. Magn. Reson.* **1995**, *115*, 197.
(4) Geerlings, J. D.; Varma, C.; van Hermet, M. C. *J. Phys. Chem. B* **2000**, *104*, 56.
(5) Horng, M. L.; Gardecki, J. A.; Papazyan, A.; Maroncelli, M. *J. Phys. Chem.* **1995**, *99*, 17311.
(6) Gardecki, J.; Horng, M. L.; Papazyan, A.; Maroncelli, M. *J. Mol. Liq.* **1995**, *65*−*6*, 49.
(7) Khajehpour, M.; Kauffman, J. F. *J. Phys. Chem.* A **2001**, *105*, 10316.
(8) Ladanyi, B. M.; Perng, B. C. *J. Phys. Chem.* A **2002**, *106*, 6922.
(9) Ladanyi, B. M.; Maroncelli, M. *J. Chem. Phys.* **1998**, *109*, 3208.
(10) Ingrosso, F.; Ladanyi, B. M.; Mennucci, B.; Elola, M. D.; Tomasi, J. *J. Phys. Chem. B* **2005**, *109*, 3553.
(11) Ingrosso, F.; Ladanyi, B. M.; Mennucci, B.; Scalmani, G. *J. Phys. Chem. B* **2006**, *110*, 4953.
(12) Frisch, M. J.; et al. *Gaussian 2003*, revision B.03; Gaussian, Inc.: Pittsburgh, PA, 2003.
(13) Chapman, D. A.; Hester, R. E. *J. Phys. Chem. A* **1997**, *101*, 3382.
(14) Cornell, W. D.; Cieplak, P.; Bayly, C. I.; Gould, I. R.; Merz, K. M., Jr.; Ferguson, D. M.; Spellmeyer, D. C.; Fox, T.; Caldwell, J. W.; Kollman, P. A. *J. Am. Chem. Soc.* **1995**, *117*, 5179.
(15) Jorgensen, W. L.; Maxwell, D. S.; Tirado-Rives, J. *J. Am. Chem. Soc.* **1996**, *118*, 11225.
(16) Rizzo, R. C.; Jorgensen, W. L. *J. Am. Chem. Soc.* **1999**, *121*, 4827.
(17) Watkins, E. K.; Jorgensen, W. L. *J. Phys. Chem.* A **2001**, *105*, 4118.
(18) Kumar, P. V.; Maroncelli, M. *J. Chem. Phys.* **1995**, *103*, 3038.
(19) Allen, M. P.; Tildesley, D. *Journal of Computer Simulation of Liquids*; Oxford University Press: Oxford, U.K, 1987.
(20) CRC *Handbook of Chemistry and Physics*, 73rd ed.; Lide, D. R., Ed.; CRC Press: Boca Raton, FL, 1992−1993.
(21) Cremer, D.; Pople, J. A. *J. Am. Chem. Soc.* **1975**, *97*, 1354.
(22) Davis, M.; Hassel, O. *Acta Chem. Scand.* **1963**, *17*, 1181.
(23) Buschmann, J.; Muller, E.; Luger, P. *Acta Crystallogr., Sect. C: Cryst. Struct. Commun.* **1986**, *42*, 873.
(24) Esteban, A. L.; Galache, M. P. *Mol. Phys.* **1994**, *82*, 303.
(25) Bako, I.; Palinkas, G.; Dore, J.; Fischer, H. *Mol. Phys.* **1999**, *96*, 743.
(26) Krienke, H.; Ahn-Ercan, G.; Barthel, J. *J. Mol. Liq.* **2004**, *109*, 115.
(27) Levesque, D.; Verlet, L.; Kurkijarvi, J. *Phys. Rev. A* **1973**, *7*, 1690.
(28) Holz, M.; Heil, S. R.; Sacco, A. *Phys. Chem. Chem. Phys.* **2000**, *2*, 4740.
(29) Satija, S. K.; Wang, C. H. *Chem. Phys. Lett.* **1977**, *46*, 352.
(30) Fatima, M.; Ferreira Marques, R. M.; Amorim da Costa, A. M. *J. Mol. Struct.* **1986**, *143*, 291.
(31) Fatima, M.; Ferreira Marques, R. M.; Amorim da Costa, A. M. *J. Raman Spectrosc.* **1987**, *18*, 457.
(32) Hare, M.; Rodrigues, V.; Cea, P.; Lopez, M.; Lafuente, C. *Int. J. Thermophys.* **2004**, *25*, 669.
(33) Nayak, J. N.; Aralaguppi, M. J.; Aminabhavi, T. M. *J. Chem. Eng. Data* **2003**, *48*, 1489.
(34) Cichos, F.; Brown, R.; Bopp, P. A. *J. Chem. Phys.* **2001**, *114*, 6834.
(35) Carter, E. A.; Hynes, J. T. *J. Chem. Phys.* **1991**, *94*, 5961.
(36) Fleming, G. R.; Cho, M. *Annu. Rev. Phys. Chem.* **1996**, *47*, 109.
(37) Egorov, S. A. *J. Chem. Phys.* **2000**, *113*, 1950.
(38) Reynolds, L.; Gardecki, J. A.; Frankland, S. J. V.; Horng, M. L.; Maroncelli, M. *J. Phys. Chem.* **1996**, *100*, 10337.
(39) Ladanyi, B. M. *Theoretical Methods in Condensed Phase Chemistry*; In Schwartz, S. D., Ed.; Kluwer: Dordrecht, The Netherlands, 2000.
(40) Ingrosso, F.; Tani, A.; Tomasi, J. *J. Mol. Liq.* **2005**, *117*, 85.
(41) St. Pierre, A. G.; Steele, W. A. *Mol. Phys.* **1981**, *43*, 123.
(42) Nugent, S.; Ladanyi, B. M. *J. Chem. Phys.* **2004**, *120*, 874.
(43) Ladanyi, B. M.; Nugent, S. *J. Chem. Phys.* **2006**, *124*, 044505.
(44) Ingrosso, F.; Mennucci, B.; Tomasi, J. *J. Mol. Liq.* **2003**, *108*, 21.
(45) Burnell, E. E.; De Lange, C. A. *Chem. Rev.* **1998**, *98*, 2359.
(46) Dingemans, T.; Photinos, D. J.; Samulski, E. T.; Terzis, A. F.; Wutz, C. *J. Chem. Phys.* **2003**, *118*, 7046.
(47) Rau, J.; Ferrante, C.; Kneuper, E.; Deeg, F. W.; Bräuchle, C. *J. Phys. Chem.* A **2001**, *105*, 5734.